Resolving Shallow Shear-Wave Velocity Structure beneath Station CBN by Waveform Modeling of the M_w 5.8 Mineral, Virginia, Earthquake Sequence

by Zhiwei Li, Sidao Ni, and Paul Somerville

Abstract   The 23 August 2011 M_w 5.8 Mineral, Virginia, earthquake was the largest earthquake in the central and eastern United States in the past 100 years, and it was well recorded by strong motion and broadband seismometers, thus providing abundant ground-motion data for earthquake ground-motion studies. The largest recorded ground motion among Advanced National Seismic System stations was at station CBN, but the site effects at station CBN need to be understood because the strong motions recorded there do not represent bedrock site conditions. On the radial component of these recordings, the initial P wave is very weak, and is followed by a strong signal 0.3 s later, which is interpreted to be the S wave converted from the P wave (PS) at the interface between the sediments and bedrock. We first estimate the subsurface shear-wave velocity by modeling the ratio of the radial to vertical components of the initial P waves, and then resolve the velocity structure and thickness of the unconsolidated sediments by modeling the PS wave. The subsurface shear-wave velocity is found to be approximately 300 m/s, consistent with field survey results. The shear-wave velocity at the bottom of the sediments is constrained to be in the range of $320 \sim 780$ m/s, from which the thickness of the layer is estimated to be $100 \sim 230$ m. The estimates of shear-wave velocity structure and thickness of the sediments are further improved by modeling the oscillatory waveforms between the P and S waves. This study suggests that site characterization for the estimation of ground-motion amplification at a site can be achieved inexpensively and noninvasively by modeling local P waveforms recorded at the site.

Introduction

On 23 August 2011, an M_w 5.8 earthquake occurred in Mineral, Virginia (referred to as the Mineral earthquake hereafter; Fig. 1), which is the largest earthquake in the central and eastern United States (CEUS) in the last 100 years (U.S. Geological Survey, 2011). The earthquake caused light-to-moderate damage in the surrounding region, including Washington D.C., and generated modified Mercalli intensity up to VIII in the epicentral region (Chapman, 2013). In view of the low seismic activity in the CEUS, this earthquake sequence provides a valuable dataset for earthquake ground-motion studies. However, the USArray has not covered the epicentral region yet and only a few permanent seismic stations recorded the Mineral earthquake sequence within an epicentral distance of 100 km. Among these stations, station CBN of the U.S. National Seismograph Network is the closest permanent backbone station of Advanced National Seismic System (ANSS), and about 57 km away from the Mineral earthquake. Although it is not the closest station (the nonbackbone CVVA station is the closest station with an epicentral distance of about 54 km

as shown in Fig. 1), it recorded the maximum peak ground velocity (PGV) of $0.135g$, which is ∼11% larger than the PGV of $0.121g$ at CVVA. Stronger ground motion at a more distant station could possibly be attributed to differences in site response.

Site response is mostly controlled by the subsurface shear-wave velocity structure, especially the top tens to hundreds of meters (Wald and Mori, 2000; Boore, 2004, 2006; Liu *et al.*, 2011). However, knowledge of shear-wave velocity structure down to hundreds of meters is also necessary when assessing site response (Chiu and Langston, 2011). As station CBN recorded the strongest ground motion among the backbone ANSS stations, it is important to understand the site response beneath that station to infer the ground motions that would have been recorded on rock site conditions.

Methodology

A detailed review of both active and passive methods for determining subsurface velocity structure was made by
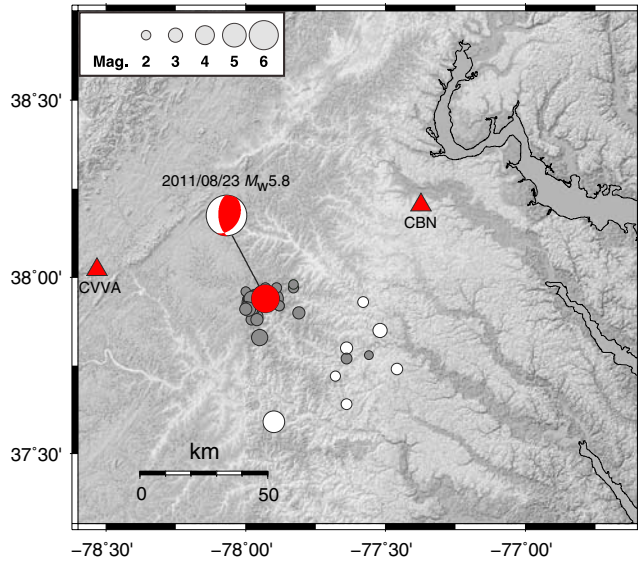
Figure 1. Topographic map of the region around the M_w 5.8 Mineral earthquake. Triangles show the location of station CBN. Circles indicate the earthquakes from 2001 to 2012. White and gray circles show the earthquakes before and after the mainshock. The color version of this figure is available only in the electronic edition.

Boore (2006). Proxy methods such as slope, terrain, and mapped surface geology have also been proposed for characterizing site effects (Wald and Allen, 2007; Kottke *et al.*, 2012; Yong *et al.*, 2012). In this paper, we use a newly developed method to study the shallow shear-wave velocity structure with three-component local earthquake *P* waves. From a theoretical derivation (Aki and Richards, 2002; Ni, 2011; B. Kim *et al.*, unpublished report, 2013; Ni *et al.*, 2014), it has been demonstrated that the amplitude ratio of radial to vertical initial *P* waves is a good indicator of subsurface shear-wave velocity. The radial/vertical amplitude ratio at the surface can be represented as

$$Ur/Uz = \frac{2\beta p \cos j}{1 - 2p^2\beta^2}, \quad (1)$$

in which β is shear-wave velocity, p is the ray parameter, j is the angle of reflected *S* wave, and Ur and Uz are the displacements of the radial and vertical components. Noting that $\cos j = \sqrt{1 - (\beta p)^2}$, we see that the shear-wave velocity β can be determined based on equation (1):

$$\beta = \frac{1}{p}\sqrt{\frac{1 - \sqrt{\frac{1}{1+(Ur/Uz)^2}}}{2}}. \quad (2)$$

Therefore, shear-wave velocity β can be estimated directly from the Uz/Ur ratio and the ray parameter p. This approach has been validated for ANSS stations in the CEUS (B. Kim *et al.*, unpublished report, 2013).

Moreover, for the case of unconsolidated sediment overlying hard rock, the incoming *P* wave can be converted to an *S* wave named *PS* (Langston, 2003a) due to the sharp contrast between sediment and bedrock. When the source dura-

tion of a local earthquake is short enough (which is usually the case for small-to-moderate earthquakes), the direct *P* wave and the *PS* wave can be observed as isolated pulses on the radial component. The amplitude of *PS* and its time lag after the *P* wave provide extra constraints on the shear-wave velocity of the sediments. For example, the velocity structure of unconsolidated sediments in the Mississippi embayment is resolved by modeling the timing and strength of *PS* from local earthquakes (Chiu and Langston, 2009, 2011) although attenuation parameters could not be estimated (Langston, 2003b).

Data

Station CBN is equipped with both broadband seismometers and accelerographs. At epicentral distances of about 60 km, high-quality waveform data have been recorded at CBN from tens of local earthquakes including the Mineral earthquake and its aftershocks. We collected these seismic waveforms recorded at CBN from local earthquakes that occurred between January 2001 and June 2012 (Fig. 1; Table A1). For the mainshock, velocity seismograms are computed from strong-motion data (acceleration, HN channel) at station CBN because the broadband records (BH channel) clipped. The source parameters of the 2011 M_w 5.8 Mineral earthquake are also shown in Table A2. As displayed in Figure 2, direct *P* and *PS* waves are clearly observed on these local waveforms (**M** 2–**M** 4 for aftershocks). The first pulse of the *P* waves on the radial component is much weaker than that on the vertical component, suggesting that the subsurface shear-wave velocity (V_S) is very low (from equation 1, the lower the V_S, the weaker the *P* wave on the radial component). Moreover, as shown in Figure 3a, there is a strong secondary arrival about 0.3 s after the *P* wave on the radial component. The secondary arrival is even stronger than the direct *P* wave. Good coherence of the radial and vertical waveforms can be achieved with a time shift of ~0.3 s on the radial component. Their almost identical waveforms suggest that the strong secondary arrival on the radial component is converted from the *P* wave at a sharp interface. We propose that the strong secondary arrival is the *PS* wave from the boundary between unconsolidated sediments and hard bedrock, because similar features are observed in the Mississippi embayment (Langston, 2003a). The *PS*/*P* amplitude ratio is measured with the cross-correlation method, and is found to be in the range of 1.3 ∼ 1.5 (Fig. 3b).

To resolve the subsurface shear-wave velocity and depth of the sharp interface, we compute synthetic seismograms and compare them with observed waveform data. Synthetic displacement waveforms can be calculated by double integration in the frequency–wavenumber domain (*f*-*k*; Zhu and Rivera, 2002) or by single integral in the frequency domain by the reflection matrix approach using a plane-wave approximation (plane-wave method; Haskell, 1960; Kennett, 1983; Randall, 1989). The latter approach is adopted for computing synthetic seismograms for the *P* waves because
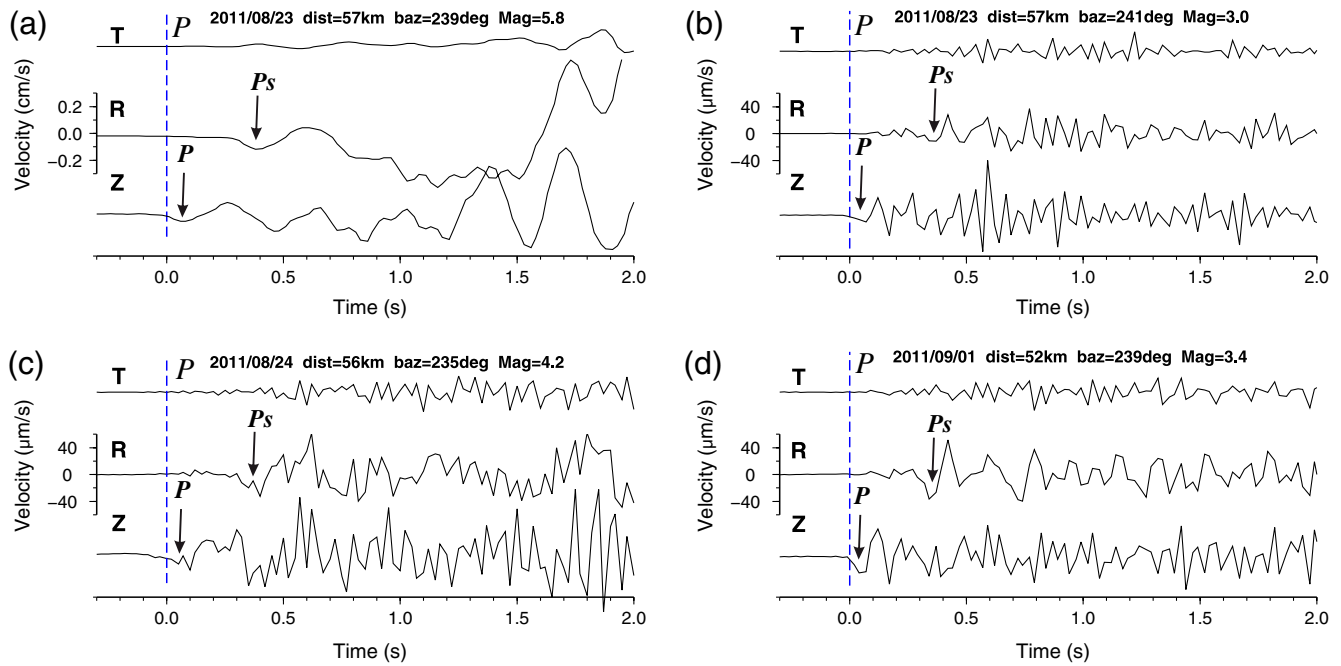
Figure 2. Radial (R), vertical (Z), and tangential (T) components of seismograms of (a) mainshock and (b–d) aftershocks of the Mineral earthquake at station CBN. The data have been transformed into velocity waveforms by removing instrument response. Clear *PS* phases can be observed 0.3 s after the *P* wave. First *P* arrivals are labeled on each waveform. The origin time, epicentral distance, and magnitude of each earthquake are labeled on each panel. The color version of this figure is available only in the electronic edition.
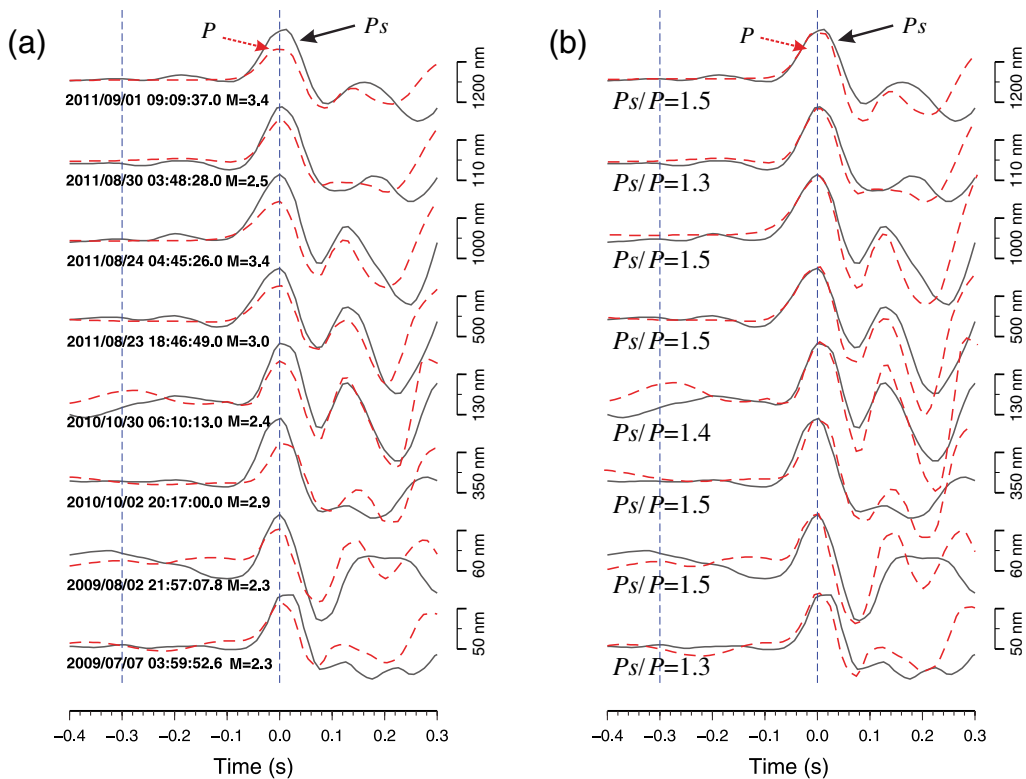
Figure 3. Comparison between radial components (solid line) shifted 0.3 s forward and vertical components (dashed line). (a) Radial and vertical components plotted on the same scale. (b) Vertical components magnified to match radial component amplitudes. Magnification factors are indicated below each seismogram. Good coherence between radial and vertical components suggests the radial components are converted from the *P* wave on the vertical components (*PS*). The color version of this figure is available only in the electronic edition.
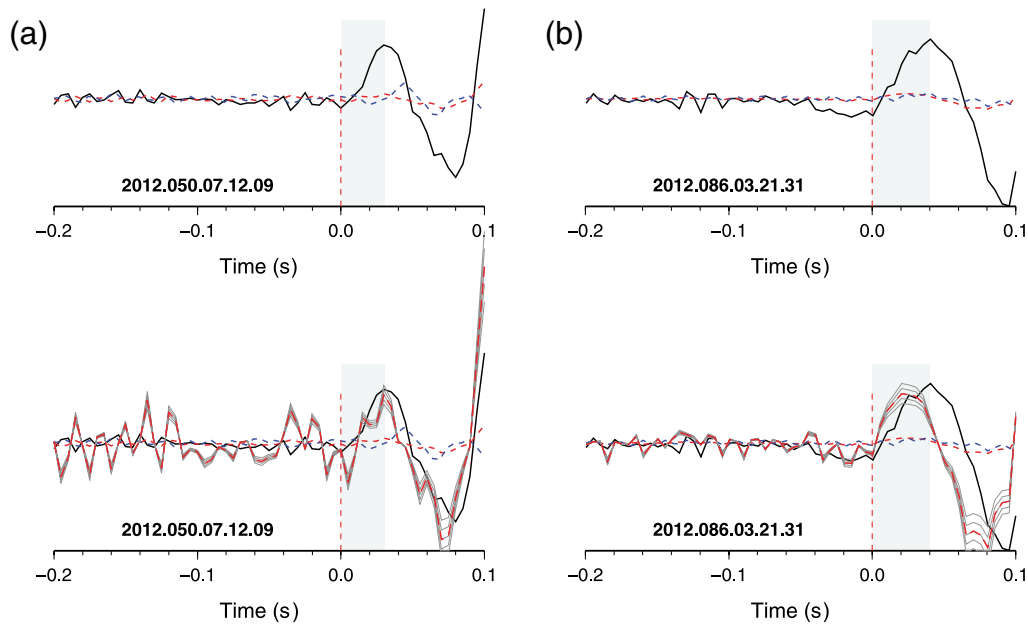
Figure 4. Vertical (solid black line), radial (dashed-dotted line), and tangential (dotted line) component waveforms of (a) 19 February 2012 **M** 2.7 and (b) 26 March 2012 **M** 3.1 aftershocks of the 23 August 2011 Mineral earthquake. Upper panel shows the three components plotted on the same scale. Bottom panel shows the radial components amplified by factors of 8, 9, 11, 12 (gray lines), and 10 (dashed line). The Uz/Ur ratio approximately equals 10. The gray bars show the approximate time window from first arrival to the maximum amplitude of the P wave. The waveform sampling rate is 200 samples per sec. The color version of this figure is available only in the electronic edition.

of its much higher speed. As confirmed by Ni *et al.* (2014), the first 1 second segments of the P waveforms calculated using the plane-wave approximation are consistent with those from the f-k method for epicentral distances of several tens of kilometers. Thus, due to its computational efficiency, we adopt the plane-wave method in computing the synthetic seismograms.

## Analysis of the Subsurface Shear-Wave Velocity and Thickness of the Unconsolidated Sediment

From equation (1), we determine the surface shear-wave velocity at station CBN using the radial/vertical amplitude ratio (Uz/Ur) of the initial P waves (Fig. 4). The broadband seismic waveforms (channel BHZ, BHN, and BHE) of the CBN recording are digitized at 40 samples per sec, which is not sufficient for higher-temporal resolution of the Uz/Ur ratio of P wave. In order to estimate the shear-wave velocity of the surface sediments, we made the measurement on the P waves from the broadband, high-sample rate (200 samples per sec) component data stream (channel HNZ, HN1, and HN2). The Uz/Ur ratio of the P wave is measured by visual inspection, comparing the first wiggle of the P wave on the radial component, magnified by factors from 5 to 20, with the first wiggle of the P wave on the vertical component.

The slowness of the P wave (p in equation 1) is computed from the 1D CEUS crustal model (Table A3) assuming the hypocenter location and focal depth estimated by Chapman (2013), and is found to be approximately 0.16 s/km. As

shown in Figure 4, the Uz/Ur ratios of the P wave from two aftershocks are approximately 10, which, together with the measurements of another four aftershocks (not shown in the figure), indicate that the surface shear-wave velocity ($V_{S_{top}}$) is in the range of 260–380 m/s with an average value of ~300 m/s. The source durations of the three local earthquakes are 0.1 s or less, suggesting the depth resolution below the ground surface of this surface velocity measurement is ~30 m or less according to the equation for estimating depth resolution assuming 0.1 s × V_S (Ni *et al.*, 2014).

Although the subsurface V_S can be estimated from the Uz/Ur ratio of the initial P waves, the V_S at the bottom of the sediments ($V_{S_{bottom}}$) can be inferred from the PS/P ratio (defined as the ratio between the PS amplitude on the radial component and the initial P-wave amplitude on the vertical component; Langston, 2003a; Chiu and Langston, 2011). To explore how the PS/P ratio depends on the velocity contrast, we measured the PS/P ratio from the PS phase on the radial component and the P phase on the vertical component of synthetic seismograms, which are computed with the plane-wave approximation.

A velocity model, ray parameter p, and source–time function are needed for computing the synthetic seismograms. The velocity model used in the moment tensor solution of Saint Louis University (referred to as the CEUS model) is adopted as a reference model for bedrock beneath the unconsolidated sediment at station CBN (Table A3). Ray parameter p is also computed with the CEUS model for a focal depth of 6 km and epicentral distance of 52 km.
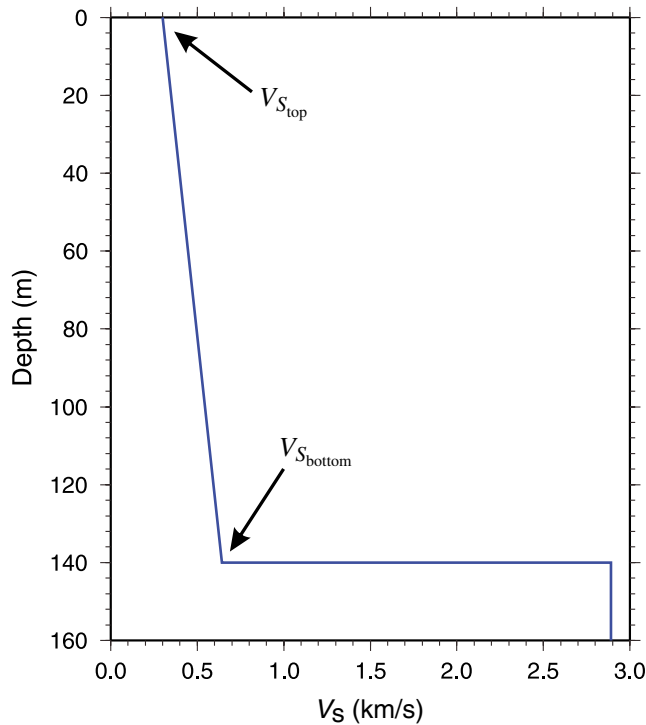
Figure 5. Schematic model for the unconsolidated sediments beneath station CBN. Shear-wave velocity increases linearly with depth in the sediment, and P velocity is fixed at 1525 m/s. The color version of this figure is available only in the electronic edition.

The source–time function is a Gaussian function with duration of 0.1 s. The P-wave velocity in the sediments is also needed for computing PS/P ratio, and we adopt a P velocity model of the sediment layer with homogeneous $V_P = 1.525$ km/s measured from a field refraction survey (Martin, 2013). The shear-wave velocity in the sediments is assumed to increase linearly with depth (Fig. 5). The subsurface shear-wave velocity ($V_{S_{top}}$) is set to 300 m/s according to the measurement of the Uz/Ur ratio of the P wave described above.

We compute synthetic seismograms for different $V_{S_{bottom}}$, and then measure the PS/P ratio. In Figure 6, we display overlain PS and P waves for $V_{S_{bottom}}$ of $300 \sim 800$ m/s. It is observed that the PS/P amplitude ratio is larger when $V_{S_{bottom}}$ increases (Fig. 6). The theoretical PS/P amplitude ratio is also displayed in Figure 7. As the measured PS/P amplitude ratio is in the range of about 1.3–1.5, the $V_{S_{bottom}}$ is thus estimated to be in the range of $320 \sim 780$ m/s. However, the PS/P amplitude ratio measurement is not very accurate and can only provide moderate constraints on $V_{S_{bottom}}$ because PS is a secondary arrival and its waveform is contaminated. For example, there are negative pulses before PS for some **M** 2+ earthquakes (Fig. 3). Thus, the thickness of the sedimentary layer is estimated to be $100 \sim 230$ m from the time interval between PS and P (which is 0.3 s as shown in Fig. 3), with the $V_{S_{top}}$ ($260 \sim 380$ m/s) constrained from the Ur/Uz amplitude ratio of the initial P wave and $V_{S_{bottom}}$ ($320 \sim 780$ m/s) constrained from PS/P amplitude ratio.

Discussion and Conclusions

Local earthquake waveforms have demonstrated potential for estimating the shallow shear-wave velocity structure in many studies. For example, the waveforms and arrival times of P- and S-wave reverberations (e.g., PS, Sp, $PpPhp$) within the sedimentary column provide useful information on the velocity structure (Kruger, 1994; Chen et al., 1996; Langston 2003a,b; Chiu and Langston 2009, 2011). However, the trade-offs between the layer parameters (e.g., layer thickness and velocity) in the study of velocity structure have also been widely recognized (Langston 2003a,b; Chiu and Langston, 2009, 2011).

The ratio Uz/Ur of the P wave used in this study provides estimates of the absolute shear-wave velocity of the uppermost surface if the ray parameter p is known. From equation (2), it is observed that only the product between the shear-wave velocity β and ray parameter p is resolvable from the Uz/Ur amplitude ratio. Therefore, substantial trade-off exists between shear-wave velocity β and ray parameter p. For example, 10% error in ray parameter readily translates into $\sim$10% error in shear-wave velocity β. The measurement of Uz/Ur and the estimate of the ray parameter p will affect the accuracy of shear-wave velocity estimates. When Uz/Ur is large ($\gg 1$), equation (2) can be approximated as equation (3):

$$\beta = \frac{1}{2p(Uz/Ur)}. \qquad (3)$$

Therefore, the error in β also depends on the inaccuracy of Uz/Ur in a similar way to ray parameter p. When the subsurface shear-wave velocity is lower than 200 m/s, Uz/Ur is greater than $\sim$15, suggesting that the amplitude of the P wave on the radial component is very small, and noise on the radial component may hinder accurate measurement of Uz/Ur. Therefore, high signal-to-noise ratio is needed for accurate Uz/Ur estimation, and **M** 3+ earthquakes recorded on local quiet stations are usually needed.

The calculation of ray parameter could be affected by earthquake mislocation and bias in the crustal velocity model. To investigate the variability of ray parameter due to uncertainty in focal depth and epicenter location of the local earthquakes recorded at CBN, we calculate ray parameter for the cases of epicentral distance of 52 km but varying focal depth from 2 to 8 km, and focal depth of 5 km but varying epicentral distance from 47 to 57 km. It is found that the ray parameter varies from 0.1624 to 0.1639 s/km, so the error in estimating subsurface velocity is small ($\sim$1%) given the small variability ($\sim$1%) in ray parameter, suggesting negligible influence on shear-wave velocity estimation.

However, we have assumed a 1D layered model in estimating the velocity structures described above, and 3D
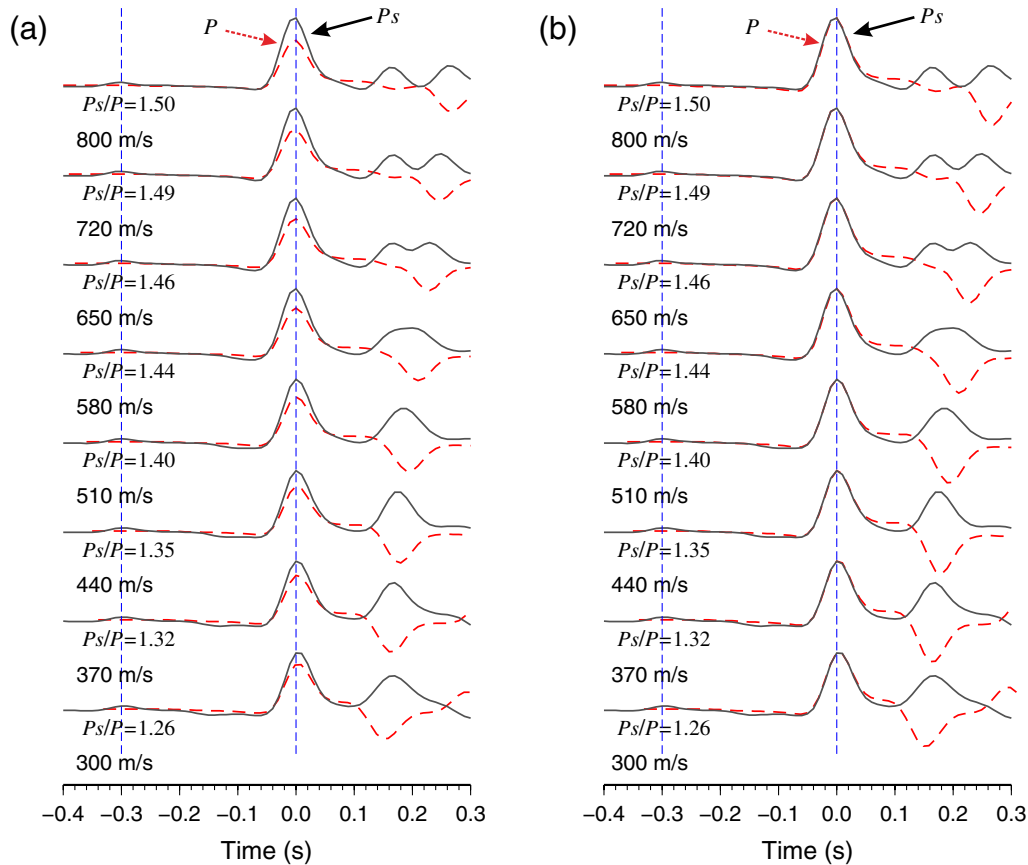
Figure 6. (a) Waveform comparisons between synthetic *PS* on the radial component (solid line) and *P* on the vertical component (dashed line) for a series of $V_{S_{bottom}}$. (b) Similar to (a), but the vertical components are magnified to match the radial components. Magnification factor and $V_{S_{bottom}}$ are indicated below each trace. The color version of this figure is available only in the electronic edition.
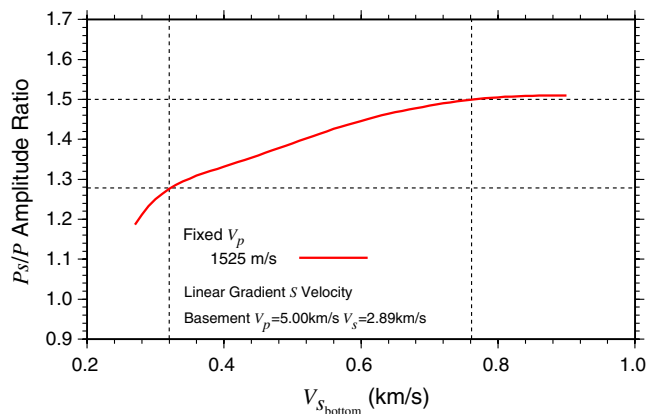

Figure 7. Theoretical *PS/P* amplitude ratio versus $V_{S_{bottom}}$. $V_{S_{top}}$ is set to be 300 m/s. Horizontal lines indicate range of observed *PS/P* amplitude ratio and the vertical lines indicate inferred $V_{S_{bottom}}$. The color version of this figure is available only in the electronic edition.

structure may affect the results by changing the ray parameter p. The Uz/Ur of local *P* waves measured from events along different azimuths may average out the 3D effect. The sensitivity of the depth extent of the surface layer to the aver-

age shear-wave velocity using the Uz/Ur ratio is approximately proportional to the source duration time, that is, the depth extent is in the range of source duration multiplied by the subsurface shear-wave velocity (Langston, 2003a; Ni *et al.*, 2014).

Furthermore, there is severe trade-off between sediment thickness and $V_{S_{bottom}}$ when the differential time between *PS* and *P* is used to estimate sediment thickness. The oscillatory waveforms between *P* and S arrivals (Fig. 8) may provide further constraints on sediment thickness and shear-wave velocity structure. We try to resolve optimal $V_{S_{bottom}}$ using a constrained grid-search algorithm. That is, $V_{S_{top}}$ is set to be 300 m/s, $V_{S_{bottom}}$ is searched in the range of 300–800 m/s in intervals of 10 m/s, whereas sediment thickness is computed with the constraint of a 0.3 s interval between *PS* and *P*. For each model, we calculate full synthetic waveforms of the Mineral earthquake at station CBN with the *f-k* method (Zhu and Rivera, 2002) assuming a double-couple source mechanism (see Data and Resources for reference). Then we compute the mismatch between observed and synthetic oscillatory waveforms between *P* and S arrivals.

From Figure A1, it is observed that smaller $V_{S_{bottom}}$ leads to a better waveform match. Usually, shear-wave velocity in
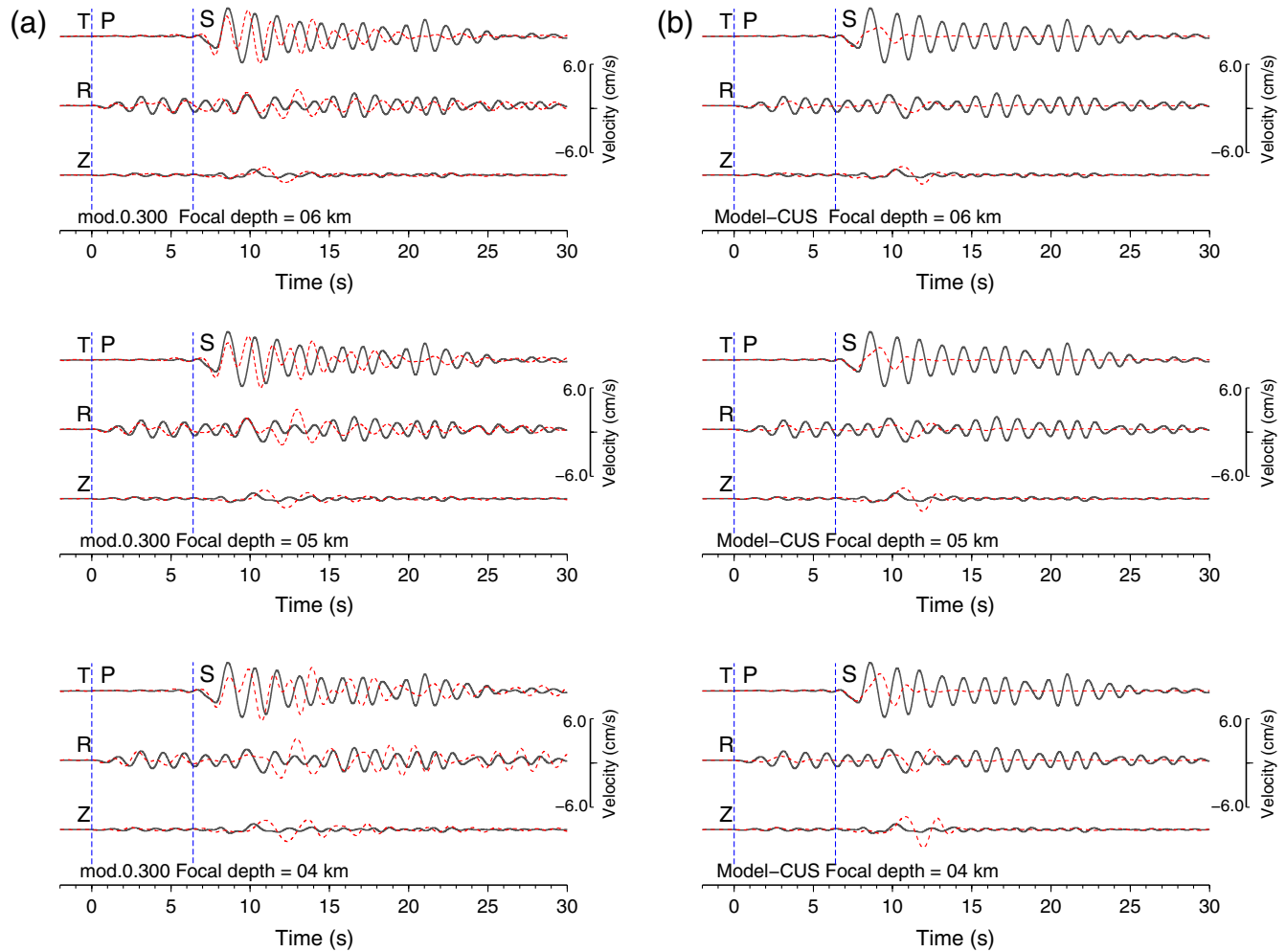
Figure 8. Synthetic (dashed line) and observed (solid line) waveforms of the Mineral earthquake at station CBN. Synthetic waveforms are calculated from (a) model mod.0.300 ($V_{S_{bottom}}$ is 300 m/s) and (b) model-CUS. A band-pass filter of $0.05 \sim 1$ Hz is used for all waveforms. Focal depths (4, 5, and 6 km) used in the computation are indicated on each panel. The color version of this figure is available only in the electronic edition.

sediments increases with depth, thus $V_{S_{bottom}}$ is probably as low as 300 m/s. With $V_P = 1525$ m/s, the sediment thickness is estimated to be about 110 m from the 0.3 s interval between P_S and P. Of course, a sediment layer 110 m thick with constant shear-wave velocity of 300 m/s (referred to as mod.0.300) is an oversimplified velocity model for site characterization of station CBN. Nonetheless, this simple velocity model can explain two major features of the mainshock seismograms at station CBN (Fig. 8). First, mod.0.300 predicts strong oscillatory wiggles on the radial component between the first P and S arrivals substantially better than the CEUS model. Second, the maximum amplitude of the tangential waveforms from mod.0.300 agrees with the observations very well. In contrast, the CEUS model underestimates the tangential amplitude by a factor of 2. Because the source parameters (such as M_w and fault plane solution) of the mainshock are well resolved from abundant broadband seismic stations (Chapman, 2013), the factor of 2 underestima-

tion of the tangential amplitude may be due to the lack of an unconsolidated sediment layer in the CEUS model. That is to say, the seismic recordings at CBN are amplified by a factor of 2 by the sediment layer. Therefore, the ground-motion data at CBN need to be calibrated for site conditions before being used to represent rock site conditions. Usually, amplification effects are frequency dependent, and the factor of 2 amplification mentioned above is probably valid for frequencies around 1 Hz. As the quality factor (Q) of the shallow crust in the study region is not well resolved yet, we only compare observed and synthetic waveforms for the frequency band of 1 Hz and lower. In conclusion, using local P-wave waveforms from the Mineral earthquake sequence and nearby earthquakes, a subsurface shear-wave velocity (~300 m/s) at station CBN is estimated by measuring the ratio of vertical to radial components of the P wave (Uz/Ur). This result is consistent with the V_{S30} result (269–274 m/s) at CBN station estimated by Electric Power

Research Institute (EPRI) using multichannel analysis of surface waves or spectral analysis of surface waves methods (Martin, 2013). Based on our study and Martin (2013), the CBN station belongs to site class *D* according to the National Earthquake Hazards Reduction Program (NEHRP) site classification (183 m/s $< V_{S30} \leq$ 366 m/s; Table A4). Of course, subsurface velocity models from field surveys may be more accurate than those from our approach. However, this case study at station CBN indicates our noninvasive, low-cost single-station method could be helpful for inferring site response using the *P* waveforms from **M** 2–**M** 4 local earthquakes recorded by the USArray and ANSS stations in the CEUS. Thus, site characterization for the estimation of ground-motion amplification may be achieved inexpensively and noninvasively by modeling local *P* waveforms.

Data and Resources

Moment tensor solutions for the Mineral earthquake and its aftershocks and the crustal velocity model (CEUS) beneath the sediment layer used in this study were obtained from http://www.eas.slu.edu/eqc/eqc_mt/MECH.NA/20110823175105/index.html (last accessed May 2013). The above website is maintained by Robert Herrmann. The maximum peak ground velocity at the nonbackbone CVVA station was obtained from http://www.strongmotioncenter.org/ (last accessed May 2013). Seismic waveform data used in this study were obtained from the Incorporated Research Institutions for Seismology (IRIS) Data Management Center.

Acknowledgments

References

Aki, K., and P. G. Richards (2002). *Quantitative Seismology*, Second Ed., University Science Books, Sausalito, California, 700 pp.

Boore, D. M. (2004). Estimating $V_S(30)$ (or NEHRP site classes) from shallow velocity models (Depth < 30 m), *Bull. Seismol. Soc. Am.* **94,** 591–597.

Boore, D. M. (2006). Determining subsurface shear-wave velocities: A review, *Third International Symposium on the Effects of Surface Geology on Seismic Motion*, Grenoble, France, 30 August–1 September 2006, 67–85.

Chapman, M. C. (2013). On the rupture process of the 23 August 2011 Virginia earthquake, *Bull. Seismol. Soc. Am.* **103,** no. 2, 613–628.

Chen, K., J. Chiu, and Y. Yang (1996). Shear-wave velocity of the sedimentary basin in the upper Mississippi embayment using S-to-P converted waves, *Bull. Seismol. Soc. Am.* **86,** no. 3, 848–856.

Chiu, S. C., and C. A. Langston (2009). Reflection and transmission imaging of the upper crust using local earthquake seismograms, *Bull. Seismol. Soc. Am.* **99,** no. 5, 3039–3054.

Chiu, S. C., and C. A. Langston (2011). Waveform inversion for one-dimensional near-surface structure in the New Madrid seismic zone, *Bull. Seismol. Soc. Am.* **101,** no. 1, 93–108.

Federal Emergency Management Agency (FEMA) (2003). NEHRP recommended provisions for seismic regulation for new buildings and other structures, *FEMA 450-1*, 309 pp.

Haskell, N. A. (1960). Crustal reflection of plane *P* and *SV* waves, *J. Geophys. Res.* **67,** 4751–4767.

Kennett, B. L. N. (1983). *Seismic Wave Propagation in Stratified Media*, Cambridge University Press, Cambridge, England, 342 pp.

Kottke, A. R., Y. Hashash, J. P. Stewart, C. J. Moss, and S. Nikolaou (2012). Development of geologic site classes for seismic site amplification for central and eastern North America, *Fifteenth World Conference on Earthquake Engineering*, Lisboa, Portugal, 24 September 2012, 1–10.

Kruger, F. (1994). Sediment structure at GRF from polarization analysis of *P* waves of nuclear explosions, *Bull. Seismol. Soc. Am.* **84,** no. 1, 149–170.

Langston, C. A. (2003a). Local earthquake wave propagation through Mississippi Embayment sediments, Part I: Body wave phases and local site responses, *Bull. Seismol. Soc. Am.* **93,** no. 6, 2671–2679.

Langston, C. A. (2003b). Local earthquake wave propagation through Mississippi Embayment sediments, Part II: Influence of local site velocity structure on Qp–Qs determination, *Bull. Seismol. Soc. Am.* **93,** no. 6, 2685–2702.

Liu, Y. Y., J. J. Chong, and S. D. Ni (2011). Near surface wave velocity structure in Chinese capital region based on borehole seismic records, *Acta Seismol. Sinica* **33,** 342–350.

Martin, A. (2013). EPRI (2004, 2006) Ground-Motion Model (GMM) review project: Shear wave velocity measurements at seismic recording stations, Electric Power Research Institute, *Technical Report, B-345*.

Ni, S. D. (2011). Estimating site response by constraining shallow velocity structure with local *P* waves. *AGU Fall Meeting, S32A01*.

Ni, S. D., Z. W. Li, and P. Somerville (2014). Estimating subsurface shear velocity with radial and vertical ratio of local *P* waves, *Seismol. Res. Lett.* **85,** no. 1, 82–90.

Randall, G. E. (1989). Efficient calculation of differential seismograms for lithospheric receiver functions, *Geophys. J. Int.* **99,** 469–481.

U.S. Geological Survey (2011). Magnitude 5.8, Virginia, http://earthquake.usgs.gov/earthquakes/eqinthenews/2011/se082311a/ (last accessed November 2013).

Wald, D. J., and T. I. Allen (2007). Topographic slope as a proxy for seismic site conditions and amplification. *Bull. Seismol. Soc. Am.* **97,** no. 5, 1379–1395.

Wald, L. A., and J. Mori (2000). Evaluation of methods for estimating linear site-response amplifications in the Los Angeles region, *Bull. Seismol. Soc. Am.* **90,** S32–S42.

Yong, A., S. E. Hough, J. Iwahashi, and A. Braverman (2012). A Terrain-based site-conditions map of California with implications for the contiguous United States, *Bull. Seismol. Soc. Am.* **102,** no. 1, 114–128.

Zhu, L., and L. A. Rivera (2002). A note on the dynamic and static displacements from a point source in multi-layered media, *Geophys. J. Int.* **148,** 619–627.

Appendix

The parameters of the earthquakes (Table A1 and A2), crustal velocity model (Table A3), and the definition of National Earthquake Hazards Reduction Program (NEHRP) site classifications in terms of V_{S30} (Table A4) are included here. The grid search result for the $V_{S_{bottom}}$ of the sediment is also shown here by fitting the reverberations between *P* and *S* arrivals between synthetic and observed seismograms (Fig. A1).

Table A1

Parameters of the Earthquakes Used in This Study

Origin Time (yyyy/mm/dd hh:mm:ss JST)	Location (° N)	Location (° W)	Depth (km)	Magnitude	Distance (km)
2009/07/07 03:59:52	37.64	77.64	11.0	2.3	67
2009/08/02 21:57:07	37.93	77.58	9.0	2.3	36
2010/10/02 20:17:00	37.84	77.42	8.2	2.9	41
2010/10/30 06:10:13	37.74	77.46	4.0	2.4	53
2011/08/23 18:46:49	37.95	77.94	5.1	3.0	57
2011/08/24 04:45:26	37.93	77.99	4.9	3.4	62
2011/08/30 03:48:28	37.93	77.94	8.5	2.5	58
2011/09/01 09:09:37	37.96	77.88	4.9	3.4	52

Table A2

Source Parameters of 2011 M_w 5.8 Mineral Earthquake Used in This Study

Origin Time (yyyy/mm/dd hh:mm:ss)	Location (° N)	Location (° W)	Depth (km)	Mechanism Strike	Mechanism Dip	Mechanism Rake	Magnitude (M_w)
2011/08/23 17:51:05	37.94	77.93	6.0	28°	50°	113°	5.8

Table A3

CEUS* Crustal Velocity Model

| Thickness (km)	V_P (km/s)	V_S (km/s)
1	5.00	2.89
9	6.10	3.52
10	6.40	3.70

*Central and Eastern United States.

Table A4

Definition of NEHRP* Site Classifications in Terms of V_{S30}
(Federal Emergency Management Agency [FEMA], 2003)

Site Class	Soil Profile Name	Average Shear-Wave Velocity in Top 30 m (m/s), V_{S30}
A	Hard rock	$V_{S30} > 1524$
B	Rock	$762 < V_{S30} \leq 1524$
C	Very dense soil and soft rock	$366 < V_{S30} \leq 762$
D	Stiff soil profile	$183 < V_{S30} \leq 366$
E	Soft soil profile	$V_{S30} < 183$

*National Earthquake Hazards Reduction Program.
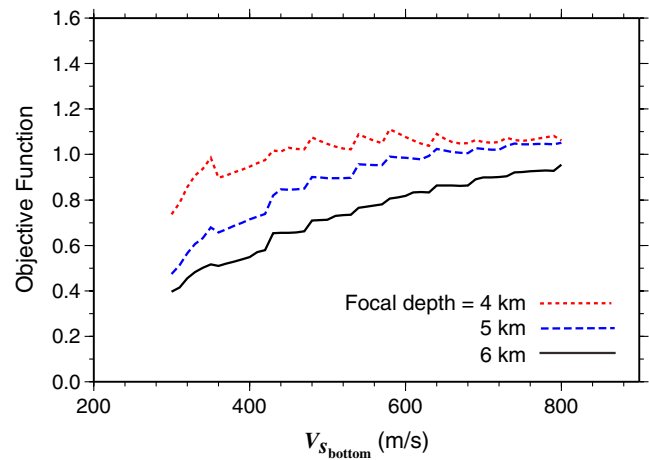
Figure A1. The objective function versus $V_{S_{bottom}}$ of the sediment. The objective function is defined as 1 CC, in which CC is the cross-correlation coefficient for the reverberations between P and S arrivals between synthetic and observed seismograms. A band-pass filter of 0.05 ∼ 1 Hz is applied for all waveforms. Dotted, dashed, and solid traces are objective functions for focal depths of 4, 5, and 6 km, respectively. Focal depth of 6 km leads to better waveform match, and smaller $V_{S_{bottom}}$ is required to fit the observation. The color version of this figure is available only in the electronic edition.

State Key Laboratory of Geodesy and Earth's Dynamics
Institute of Geodesy and Geophysics
Chinese Academy of Sciences
Wuhan 430077, China
sdni@whigg.ac.cn
    (Z.L., S.N.)

URS Corporation
Los Angeles, California 90017
    (P.S.)